https://jurnal.unimed.ac.id/2012/index.php/geo/article/view/40772
https://doi.org/10.24114/jg.v15i1.40772 - (Vol 15, No 1 - 2023)
available at http://jurnal.unimed.ac.id/2012/index.php/geo
e-issn (2549-7057) & p-issn (2085-8167)

Identification of Fault Zone in Bali Using GGMPlus Gravity and Alos-2 Palsar-2 Data

I Putu Dedy Pratama[1,2*], Takahiro Osawa[3,4], Abd. Rahman As-syakur[5,6]

[1] *Indonesian Agency for Meteorological, Climatological, and Geophysical Agency (BMKG), Indonesia*
[2]*Masters Program in Environmental Science, Udayana University, Indonesia*
[3]*Yamaguchi University International Collaboarion Office (YUICO), Udayana University, Indonesia*
[4]*Center for Research and Application of Satellite Remote Sensing (YUCARS) Yamaguchi University, Japan*
[5]*Center for Remote Sensing and Ocean Sciences (CReSOS) Udayana University, Indonesia*
[6]*Center for Environmental Research (PPLH), Udayana University, Indonesia*

ARTICLE INFO

Article History:
Received: December 04, 2022
Revision: February 02, 2023
Accepted: February 06, 2023

Keywords:
Remote Sensing
Earthquake
Derivative Gravity
Lineament
SAR

Corresponding Author
E-mail:
checkmate.mail1@gmail.com

ABSTRACT

The local active fault in Bali has a small magnitude (M<5) but has destructive potential because it is very close to residential areas. Mapping the fault area on Bali is needed to identify the parameters of faults. This study used gravity data from GGMplus, topographic data from DEMNAS, and lineaments using ALOS-2 PALSAR-2 data. Validation and interpretation using the geological map of Bali and seismicity data. We interpret the subsurface using the gravity derivative method to identify the type of fault movement. Identify fault locations using lineament extraction from SAR data processed by directional filters. The composite image red-green-blue (RGB) for HH, HV, and VV polarization was used for automatic lineament extraction and then corrected manually. The results of the gravity method succeeded in identifying 29 of the 30 faults from the geological map of the Bali sheet and a new spot from PALSAR-2. Bali land has 12 thrust faults, 11 strike-slip faults, and six normal faults. The image of PALSAR-2 (L band) has succeeded in making a fault lineament map for the Bali region. The lineament extraction results from PALSAR-2 obtained four new faults (Pesanggaran, Sepang, Tegal Badeng, and Banyuwedang), while four faults were not identified (Tampaksiring Fault, Plaga, Mambal, and Munduk-Rajasa). NE-SW dominates the strike directions, and the dip angles are 45-80 degrees. We propose 30 faults in Bali, including 26 defects from geological maps with changes in length and location shift and four new marks extracted from automatic lineament.

INTRODUCTION

Indonesian Archipelago is strongly related to quarternary plate tectonics (Verstappen, 2010). Indonesia is located at the confluence of three of the world's main tectonic plates: the Eurasian, Indo-Australian, and Pacific. Besides that, there is also the Philippine microplate, which is moving southward to the north of Sulawesi. Therefore, it is unsurprising that Indonesia's Archipelago is prone to tectonic earthquakes. As a result of tectonic processes that occur, earthquakes often occur in most parts of Indonesia. One source of the earthquake identified is the active subduction zone in the western to the eastern part of Indonesia. In addition, the remaining energy from the collision process between the plates will result in faults on land or sea in several islands and seas of Indonesia. The potential for earthquakes in Indonesia must be a concern in reducing disaster risk because it can cause fatalities. During 1815-2019, earthquakes were natural disasters that generated the highest death toll in Indonesia, with a percentage reaching 49% (Fitriyani et al., 2021).

The earthquake in Karangasem on October 15, 2021, proved that mainland Bali has several active faults. These local active faults have a small magnitude (M<5) but have the potential to damage because of their location, which is very close to residential areas. Other earthquake events, such as the Tejakula swarm in May 2017, the Kubutambahan swarm in April 2019, and most recently, the sequence of earthquakes in the Gerokgak area in February 2022, are ence of the earthquake in Bali land.

For the mainland area of Bali, there is no mention of an active fault. However, based on the geological map of the Bali sheet (Hadiwidjojo et al., 1998; Soehaimi & Setianegara et al., 2015), there are several faults and lineaments on Bali land. Based on the National Earthquake Study Center (PuSGeN, 2017) in the Bali region, the Flores Back Arc Thrust Fault in the Bali Sea and the Lombok Strait Strike-slip Fault in the Lombok Strait, east of Bali.

Conventional detection of geological lineaments in the field is costly and time-consuming, and sometimes, it is even impossible due to physical and geographical challenges (Ahmadi & Pekkan, 2021). Remote sensing has become a suitable tool for identifying large numbers of faults. Identifying faults, it can be done with data from the gravitational field, topography, and lineament patterns. Knowing the source of local earthquakes on Bali land can be a reference for earthquake-prone areas. Knowing the direction and type of fault is necessary to identify wave propagation patterns and regions with more potential for significant shaking. Mapping the fault area on the mainland of Bali using remote sensing methods is needed to identify faults on the island of Bali. The determination of the position and type of responsibility was then validated with earthquake data and geological maps. This process will produce the place, style, and model of the subsurface structure of the local fault in Bali.

This paper used gravity data from GGMplus, topographic data from DEMNAS, and lineaments using ALOS-2 PALSAR-2 data. GGMPlus has better resolution than TOPEX and BGI free-air gravity data (Suprianto et al., 2021). Compared with other gravity satellite data, the GGMplus data set offers a higher resolution (Camacho & Alvarez, 2021). In processing gravity from satellite data, topographic correction is required. Therefore DEM (Digital Elevation Model) data is needed. DEMNAS is still relatively new and has not been fully utilized for research in Indonesia (Marindah et al., 2018). Optical remote sensing data capabilities are limited due to persistent cloud coverage in the study area. Geological contours can be detected using high-resolution SAR imagery. However, effective digital processing techniques are needed to minimize inherent distortions (Ghosh et al., 2022). The l-band sensor in PALSAR-2 can penetrate the canopy of the trees, allowing us to obtain information about the ground surface, such as geological structure (Pour & Hashim, 2016).

Identifying fault patterns provides an overview of the fault location, strike, dip, and subsurface structure model on the fault. For BMKG and other related stakeholders, this information is used as a reference for the micro-earthquakes vulnerable area that has the potential to damage. For the community, this information is essential to increase awareness of the potential earthquake disasters in their area, so building construction needs to pay attention to the condition of the site and the appropriate building structure. This study will contribute preliminary information and considerations on active fault renewal from the National Earthquake Study Center (PuSGeN, 2017) on the Bali land.

RESEARCH METHODS

The research framework (Figure 1) has been designed based on the research background, which used satellite data, a seismicity catalog, and a geology map of Bali. Data division is based on processing gravity and SAR data which are then combined in interpretation with geological field surveys for some fault locations. The

data combinations are used to determine and validate the type, location, and parameters of the faults in the mainland area of Bali.

The study area is located throughout the mainland of the island of Bali (Figure 2). This study obtained quad polarization PALSAR-2 scenes from The Earth Observation Data Utilization Promotion Platform Japan (https://satpf.jp/spf/?lang=en/) for the Bali mainland area. For gravity analysis, secondary gravity anomaly data from gravimetric satellite measurements were obtained from GGMplus (http://ddfe.curtin.edu.au/gravitymodels/GGMplus/data/dg/) the form of data disturbance gravity or free air anomaly. The topographic data using the DEMNAS can be obtained from the web https://tanahair.indonesia.go.id/demnas/#/demnas. Supporting data for validation are focal mechanism data from The Global Centroid-Moment-Tensor (CMT) and the geological map of Bali from the Geological Agency, Ministry of Energy, and the Mineral Resources Republic of Indonesia.

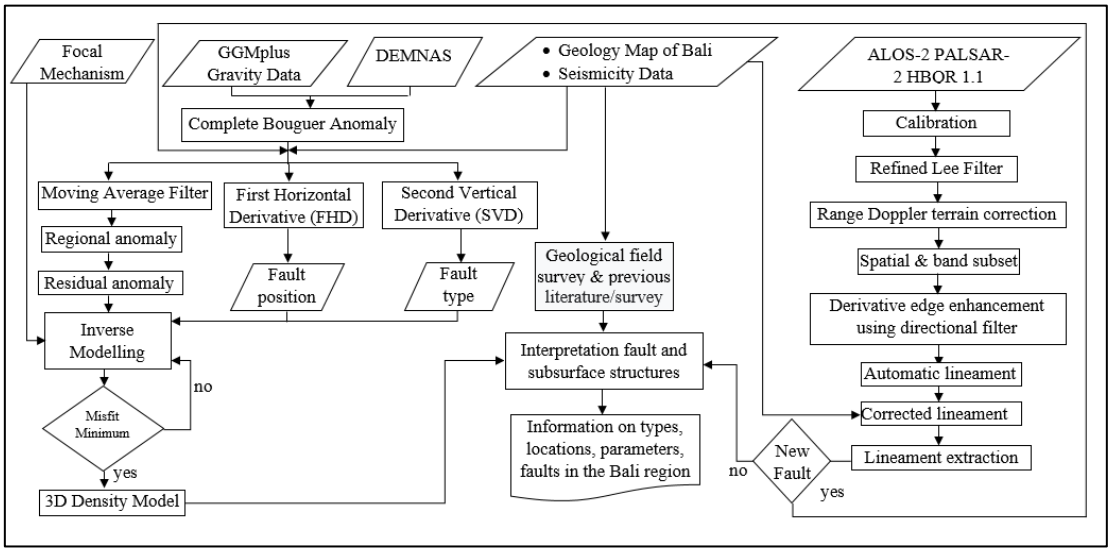

Figure 1. Research Framework

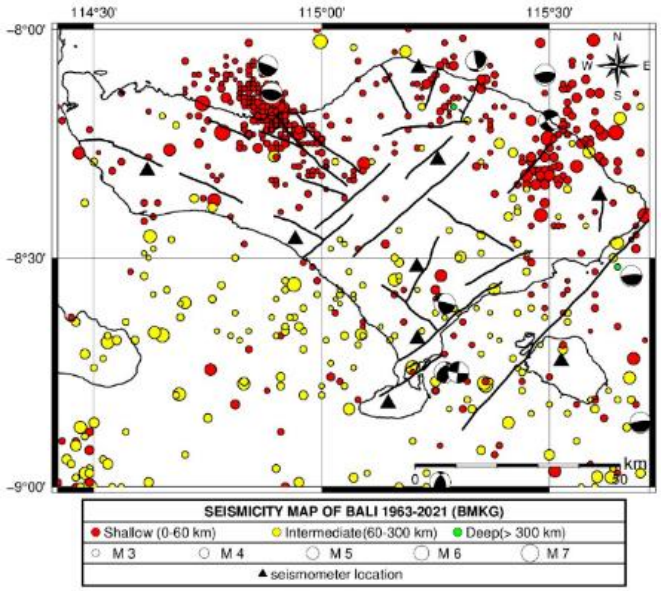

Figure 2. Distribution of Seismicity in Bali (Data catalog from BMKG 1963-2021, focal

mechanism from Global CMT, and seismometer location in Bali)

Data Collection and Preprocessing

The research data comes from gravity data from the GRACE (Gravity Recovery and Climate Experiment) and GOCE (Gravity field and steady-state Ocean Circulation Explorer) satellite measurements combined into GGMplus data (Hirt et al., 2013). This data is easy to download and greatly facilitates research compared to information with direct measurements. The downloaded GGMplus gravity data consists of Free Air Anomaly (FAA) data and DEMNAS, the altitude or topographic data.

Location and date of product created in Earth Intelligence Collection and Shearing (EICS) system on September 16, 2022. This study uses strip map full polarimetric (HH+HV+VV+VH) PALSAR-2 scenes from The Earth Observation Data Utilization Promotion Platform Japan (https://satpf.jp/spf/?lang=en) for the Bali Area (11 data). The SAR images were provided as the HBQR: High-sensitive Full (Quad.) polarimetric mode data with the processing level 1.1 (JAXA, 2014). The temporal repeat of strip map full polarimetric is one coverage per 5 years (JAXA, 2022). The data summaries of ALOS-2 PALSAR-2 in this study are shown in Table 1.

Table 1. ALOS-2 PALSAR-2 Data Summaries

No.	ID	Acquisition Date & Time	Off Nadir Angle	Data Size
1	ALOS2051537020-150507	2015-05-07 16:37:27Z	28.4	5382.4
2	ALOS2051537030-150507	2015-05-07 16:37:27Z	28.4	5382.4
3	ALOS2049467020-150423	2015-04-23 16:37:27Z	30.9	5646.1
4	ALOS2047397010-150409	2015-04-09 16:37:19Z	33.2	6913.6
5	ALOS2047397020-150409	2015-04-09 16:37:19Z	33.2	6888.2
6	ALOS2055677010-150604	2015-06-04 16:37:18Z	35.3	6522
7	ALOS2055677020-150604	2015-06-04 16:37:18Z	35.3	5382.4
8	ALOS2053607030-150521	2015-05-21 16:37:27Z	25.5	6742
9	ALOS2053607010-150521	2015-05-21 16:37:27Z	25.5	6742
10	ALOS2053607020-150521	2015-05-21 16:37:27Z	25.5	6742
11	ALOS2049467010-150423	2015-04-23 16:37:27Z	30.9	5668.1

(Source: Data Summary, 2022).

The processing includes (a) radiometric calibration, (b) speckle noise reduction using a Lee Sigma filter with 7×7 pixels window size and 0.9 sigma factor, (c) terrain correction, (d) mosaic, and (e) subset image for the Bali area. The data are geo-referenced and geo-coded data, which enables the images to be oriented so that the north direction of the observed image corresponds to the upper direction of the image (Pour & Hashim, 2015). Multilook is optional because terrain correcting was applied, and unlike the previous ALOS, ALOS-2 did not need deskewing (Veci, 2015).

Data Processing

The gravity method helps detect deep-buried structures beneath the land surface that contribute to earthquakes (Yan et al.,

2019; Choi et al., 2020). Topographic correction is required in processing gravity from satellite data; therefore, DEM (Digital Elevation Model) data is needed. The advantage of this DEMNAS data is that it has a 0.27 arc-second higher spatial resolution compared to the other DEM data resolution. The gravity anomaly data from satellite imagery is in the form of Free Air Anomaly (FAA) data, so the value of the Simple Bouguer Anomaly (SBA) and Complete Bouguer Anomaly (CBA) are expressed as:

$$SBA = FAA - BC \quad (1)$$

$$CBA = FAA - BC + TC \quad (2)$$

Where BC is Bouguer Correction, and TC is Terrain Correction. This method was performed on a Complete Bouguer Anomaly (CBA) with Oasis Montaj Software. The study area's rock mass density or rock density can be determined using the Parasnis method. This method uses the observed gravity equation in which the density component is moved to the left in the formulation. The formulation is as follows:

$$(g_{obs} - g_t + 0.3086h = (2\pi Gh)\rho + BA \quad (3)$$

Where g_{obs} is value gravity observed, tide, drift, and closing correction, g_t Is the value of theoretical gravity at the place of observation, h is the elevation of the observation point, and ρ is rock density. The moving average method averages the anomaly values. Indirectly, the moving average filter is operated by dividing by a number limit derived from an input signal to produce each limit on each output signal; the equation can be written as follows:

$$g[i] = \frac{1}{M}\sum_{j=0}^{M-1} x\,[i + j] \quad (4)$$

Where x(i,j) is the input, M is the average of the input value, and g[i] is the value of the regional anomaly. The moving average method requires window size [i,j] in the calculation process. Residual gravity anomaly is the result of simple subtraction of the Bouguer anomaly to the regional gravity anomaly in the following equation:

$$\Delta g_{residual} = \Delta g_{CBA} - \Delta g_{regional} \quad (5)$$

Nowadays, the derivatives of gravity characteristic value are commonly used to detect the source horizontal edge (Ming *et al.*, 2021). The derivative method is a method to determine local subsurface conditions. The derivative process is divided into the first horizontal derivative (FHD) and the second vertical derivative (SVD). This method enhances the near-surface effect on deeper values of the gravity anomaly (Telford et al., 2004). SVD delineates fault boundaries with oscillations between the minimum and maximum values, sliced perpendicular across each density contrast transition (Sumintadireja et al., 2018).

GGMPlus gravity data is Free Air Anomaly (FAA) data. Hence, it is necessary to calculate a Bouguer correction using the topographic of DEMNAS to get the Complete Bouguer Anomaly value which is then carried out by First Horizontal Derivative (FHD) and Second Vertical Derivative (SVD) analysis to determine the type of fault and moving average calculation to obtain residual anomaly. This residual anomaly is used to make 3D modeling to get fault dip information.

The Bali area is chiefly vegetated, which is challenging in structural field mapping. Geological contours can be detected using high-resolution SAR imagery. The wavelength of the L-band (24 cm) is relatively long among microwaves such as C-band (6 cm) and X-band (3 cm), allowing to obtain information on the ground surface, such as geological structure (Pour & Hashim, 2016). For this reason, the latest Phased Array type L-band Synthetic Aperture Radar-2 (PALSAR-2) with the full polarimetric image is needed for lineament identification. The conventional method of

geological lineament is expensive and time-consuming (Yeomans et al., 2019).

On the other hand, the traditional approach is challenging to apply due to the geographical conditions of the study area. Geological lineament mapping by remote sensing leads to determining faults. The tectonic implications are a substitution of conventional methods (Ahmadi & Pekkan, 2021) PALSAR-2 data is analyzed by preprocessing, including radiometric calibration, speckle noise reduction, and terrain correction. Furthermore, mosaics and data subsets were performed to combine 11 images for HH, HV, and VV polarization.

Table 2. Parameters used for the PCI Geomatica LINE Module

Parameter	Description	Range and Unit
	Edge detection	
RADI	Filter radius. It specifies the radius of the edge detection filter (Filter de Canny).	0–8192 (pixel)
GTHR	Gradient threshold. It specifies the point for the minimum gradient level for an edge pixel to obtain a binary image (Filter de Canny)	0–255
	Curve extraction	
LTHR	Length threshold: It specifies the minimum length of the curve to be considered as lineament	0–8192 (pixel)
FTHR	Line fitting error threshold: It specifies the maximum error (in pixels) allowed in fitting a polyline to a pixel curve	0–8192 (pixel)
ATHR	The angular difference threshold is the maximum angle between two vectors to link them.	0–90 (degrees)
DTHR	Linking distance threshold: It specifies the minimum distance between the endpoints of two vectors to be connected.	0–8192 (pixel)

(Source: Ustinov et al., 2022).

Canny edge detection is a technique for extracting structural information to reduce processed data (Canny, 1986). The preprocessed image is then subjected to a 7×7 directional filter. Then, automatic lineament extraction is performed with the PCI Geomatica LINE module (Table 2) and visual analysis for structural delimitation (Bannari et al., 2016; Ustinov et al., 2022). The automatic extraction results were validated manually by digitizing to obtain straightness results based on the PALSAR-2 image. Some field surveys and literature about geology research in Bali are used as a comparison.

Spatial domain techniques are beneficial for removing random noise (Jensen, 2015). Then semi-automatic lineament extraction is applied for lineament identification based on several digital image analysis and visual interpretation techniques. The researcher's experience and a review of previous literature results reveal that a single process may not efficiently determine the exact geological lineage excluding artifacts. Therefore, it is recommended to produce a significant tectonic-geological lineament map using the integration of automatic and manual techniques.

RESULTS AND DISCUSSION

Gravity result

Before getting the Bouguer correction value, the average density of the research area is calculated first. The straight-line gradient value obtained is the study area's average density value (ρ). There are 422.500 gravity data to calculate average density. The average density estimation method used in this study is the Parasnis Method (Equation 3), by comparing the altitude value to the free air anomaly value. Based on

this method, the Bali region has an estimated average density of 2.4 gr/cm^3 (Figure 3). This density value is similar to the research of (Astra et al., 2014) with the same method in northern Bali with the results of the average density value of 2.3961 gr/cm^3.

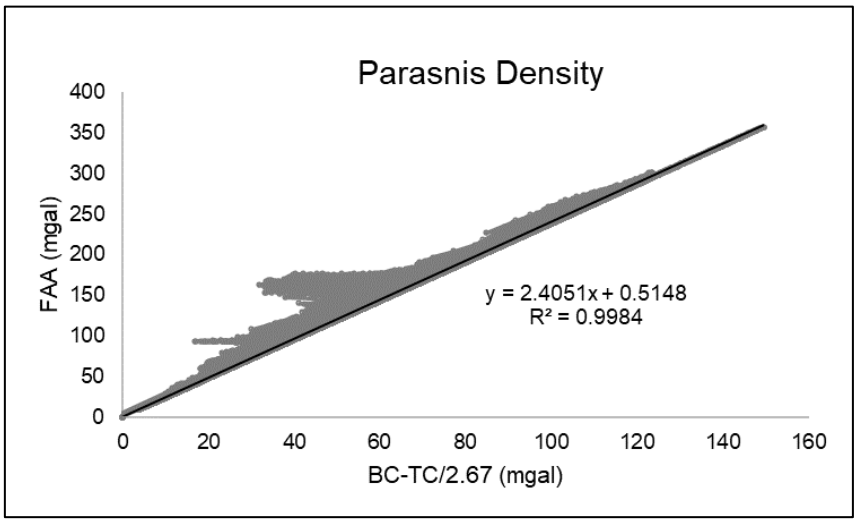

Figure 3. Average density estimation in Bali using the Parasnis method
(Source: Gravity Processing Result, 2022)

Within the perspective of 1D approximation, when |g"max| is greater than |g"min|, the anomaly corresponds to a sedimentary basin with inward-sloping edges. At the same time, if |g"max| is smaller than |g"min|, the anomaly source is a granite pluton with outward-sloping edges. Table 5.1 is the result of fault determination based on the derivative method. From the results of FHD and SVD data processing on 26 faults, it was found that ten thrust faults, 11 strike-slip faults, four normal faults, and one fault could not be identified.

Based on the residual (local) anomaly contour map in Figure 4, the Bali region has a range of values between -348,33118 mGal to 85,22365 mGal.

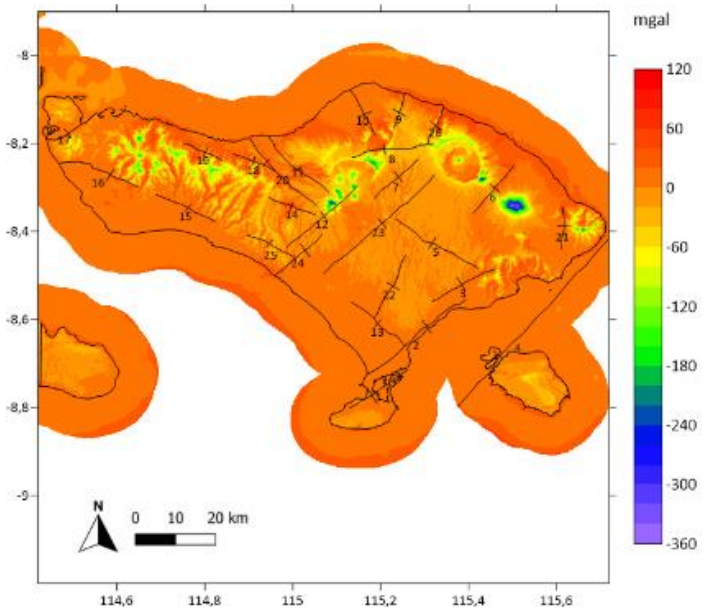

Figure 4. Residual (local) anomaly contour map of Bali
(Source: Gravity Processing Result, 2022)

Analysis of gravity data using GGMPlus found that on the island of Bali, there are all types of faults: thrust, shear, and normal. The subsurface construction by derivative method and 3D models using GGMPlus and DEMNAS data found that the strike directions are dominated by NE-SW and dip angle range from 45-80 degrees. PALSAR-2 imagery (L band) successfully created a fault lineaments map for the Bali area. NE-SW dominates the strike directions. The lineament extraction result from PALSAR-2 obtained four new faults (Pesanggaran, Sepang, Tegal Badeng, dan Banyuwedang Fault).

In comparison, four faults were not identified (Tampaksiring, Plaga, Mambal, and Munduk-Rajasa Fault). Two factors cause this: the faults are buried under the surface, and the areas are not spot zone. The presence of subduction in the south of the island of Bali, between the Eurasian Continent Plate and the Indo-Australian Ocean Plate, controls faults in Bali's land. Some spots are in the contact area of the lithological boundary, and the rest intersect the lithological boundary. Based on the age of the rock formations, these faults pass through with the age of the Quaternary rocks. All of these faults are categorized as active faults. All spots are associated with at least one earthquake occurrence and have the same fault type as their focal mechanism.

The fault in Bali is dominated by the northeast-southwest (NE-SW) strike direction with a minor northwest-southeast (NW-SE) direction. From the direction of motion, the spots in Bali are dominated by 11 strike faults, then 10 and 4 strike-slip and normal faults, respectively. The combination of gravity and SAR data can interpret marks well. However, more historical earthquake data is needed. Considering the current sensors, earthquake recording only takes time so that the fault zone will be identified appropriately. The observed image results are improving through the development of increasingly sophisticated remote sensing technology. Various methods of determining faults must be carried out, and straightforward measurements in the field must ensure each fault parameter. In the future, it is necessary to be aware of shallow earthquakes of medium-high magnitude because they can endanger residents around this fault zone, especially residents who live in houses or buildings that are not earthquake-resistant. The faults condition on the mainland of Bali land is controlled by the presence of subduction in the south of the island of Bali, between the Eurasian Continent Plate and the Indo-Australian Ocean Plate, due to the collision of these plates causing deformations on the surface of the island of Bali that mostly in East-West direction.

Figure 5 shows the fault's location along with graphical information on the analysis of the slicing FHD and SVD derivative methods in determining the fault boundaries and movement of the spot and the 3D model resulting from the Grav3D software. The color description indicates an anomaly density value from the subsurface with a range of -1,1 – 0,8 gr/cm^3. To interpret the density value, we need to add the average rock density in Bali using the Parasnis method, which is 2.4 gr/cm^3. From this anomaly range, the subsurface density ranges from 1,3 – 3,2 gr/cm^3. The dip value is obtained from interpreting the image on the density contrast boundary. The results show that modeling can still be geologically accurate and reasonable even while little input is available concerning the subsurface.

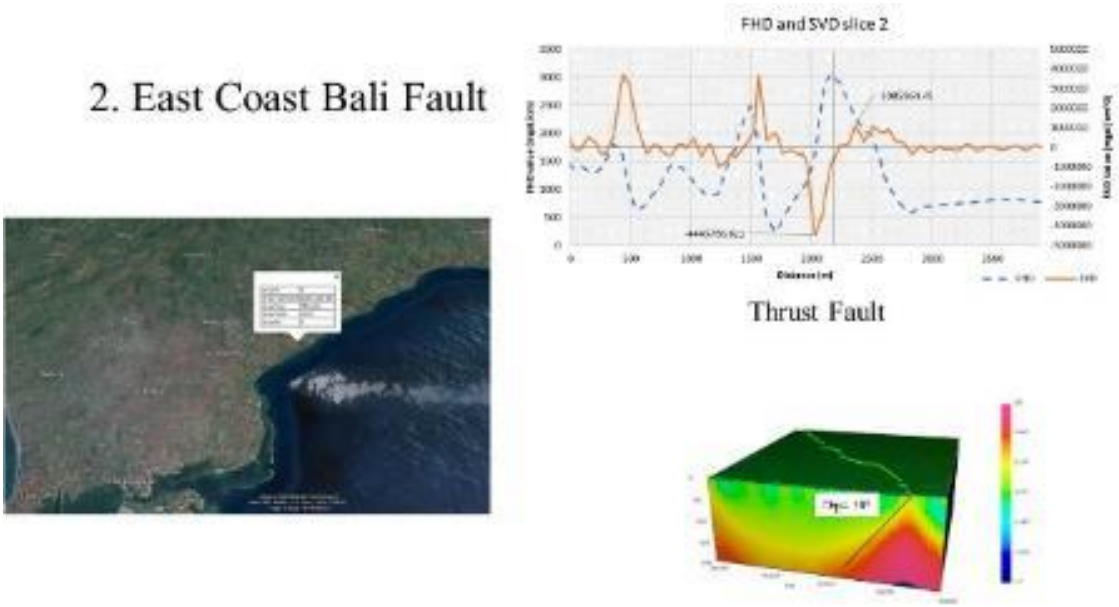

Figure 5. Representative examples of derivative gravity analysis and 3D modeling in East Coast Bali Fault (Source: Gravity Processing Result, 2022)

The GGMplus model indisputably demonstrated a higher spectral resolution in shallow cortical elements, reflected in better identification of local ingredients (Camacho & Alvarez, 2021). Gravity data processing can present fault patterns, and structures in BaliThe results of this study indicate that on the island of Bali, there are several active fault zones on land which are dominated by ascending faults, oblique faults, and several minor structures in the form of descending faults. The general direction of the upward and diagonal fault zone is NW-SE oriented, while the descending spot is found in the NE-SW order. The identified rising fault has a dip angle of 30-45, while the slope of the descending area is around 40, with a slope towards NW. The length of the fault varies between 5,7-18,6 km. All identified faults intersect Quaternary age rock. Seismic data analysis shows the association of shallow earthquake distribution with lineament patterns and geological structures. Based on the understanding that the fault structure can be categorized as an active fault if the deformation occurs in Quaternary-aged rocks and is associated with shallow seismicity, it can be interpreted that the spots identified are happening. To know the history of seismicity along these fault zones.

All identified faults cut Quaternary period rock (now-2.58 million years ago) consisting of the Holocene and Pleistocene epochs. Rocks cut by a spot indicate the relative time of fracture. The faults identified carved rocks of varying ages and sometimes penetrated the surface, which suggests that the fault is still occurring today. Based on the definition of understanding, the fault structure is categorized as an active fault if the deformation occurs in Quaternary-aged rocks and is associated with shallow seismicity (Agasya et al., 2022; Helmi et al., 2021).

SAR Result

Several combinations of threshold values were tested to identify optimal parameters for obtaining contours, and the parameters were finalized. The identified optimum parameters are as follows: RADI = 10; GTHR = 200; LTHR = 50; FTHR = 3; ATHR = 30; DTHR = 300. There are 533 lines identified automatically using the LINE module of the PCI Geomatica software with an average lineaments length of 4,3 km (Figure 6). Analysis of the strike directions

indicates that the orientation of the contours is concentrated in the northeast-southwest (NE-SW) direction.

There were 26 faults identified using PALSAR-2 data which has been carried out semi-automatic lineage extraction, including 22 faults from geological maps and four new faults with an average lineaments' length of 10,5 km (Figure 6). There are four faults from the geological map that PALSAR-2 did not identify. Of the 22 faults identified with PALSAR-2 data which is the same as the geological map, there are several differences in the length and strike of the fault.

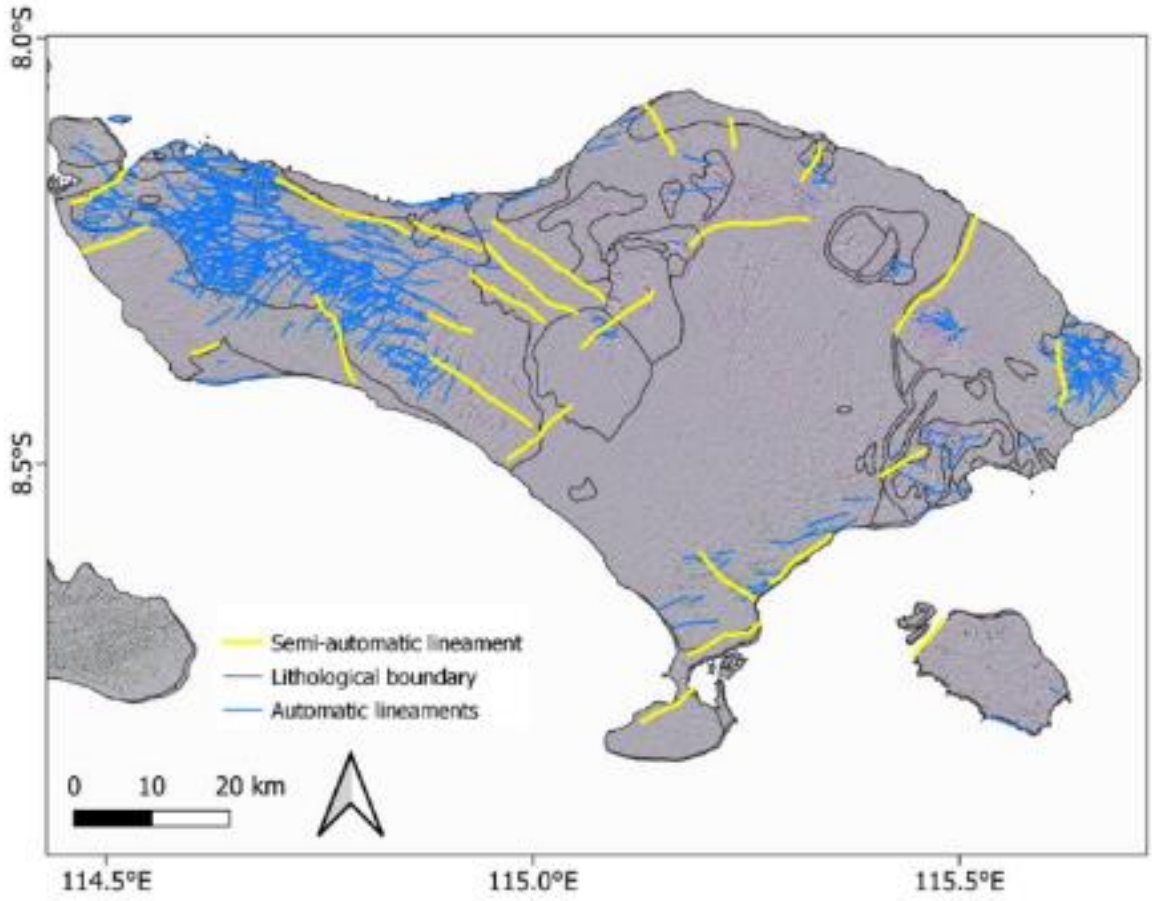

Figure 6. Lineament extraction using automatic (blue line) and semi-automatic methods (yellow line) (Source: SAR processing result, 2022)

The frequency of lineaments in different directions has been shown in Rose Diagram (Figure 7). Generally, the fault lineaments based on geological sheet maps and semi-automatic extraction results from PALSAR-2 are dominated by the northeast-southwest (NE-SW) direction. Meanwhile, the automatic extraction of PALSAR-2 is dominated by the east-west (E-W) direction. The NE-SW lineament pattern is spread across eastern and southern Bali through the Palasari Formation (QTsp) and Jembrana Volcanic (Qpvj). The NW-SE lineament pattern is spread over the east part of Bali through the contact area between the Buyan-Bratan and Batur Volcanic (Qpbb), Agung Volcanic (Qhva) and Seraya Volcanic (Qpsv) rock groups. Then in southern Bali, the lineament pattern passes through the contact area between the Buyan-Bratan and Batur Volcanic (Qpbb), Alluvium (Qa), and south formation (Tmps) rock groups.

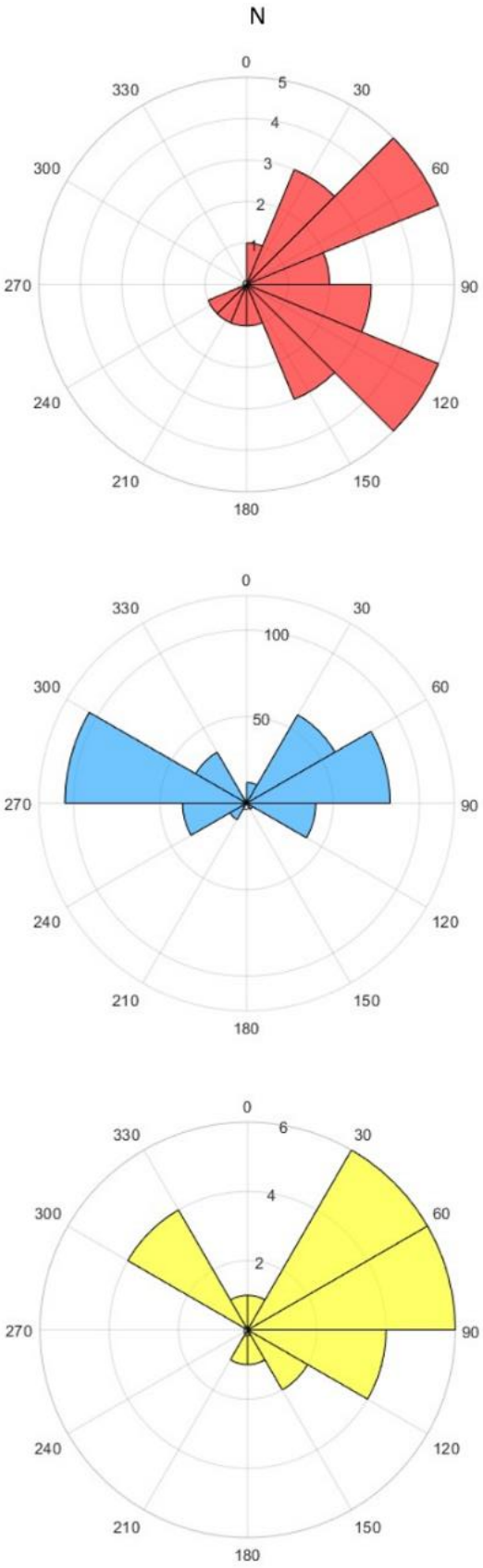

Figure 7. Rose Diagram of strike angles for fault from the geological map (red), automatic lineament extraction (blue), and semi-automatic lineament extraction (yellow). (Source: Data Processing Result, 2022)

We have plotted the frequency–magnitude relationship (Gutenberg–Richter law) using the data from an initial location with the maximum likelihood method provided in the Zmap package (Wiemer, 2001). With a reasonable magnitude of completeness (Mc) 2.3, the historical catalog of earthquakes on land in Bali will increase over time. The smaller the Mc value, the better the recording of earthquakes in the area. In addition, the development of increasingly advanced remote sensing technology will better identify faults on the island of Bali. In L-band SAR technology progress, the launch of new L-band satellites in the next few years, including ALOS-4, NISAR, and Tandem-L, will provide better and new data images to make exciting discoveries (Aoki et al., 2021). The earthquake catalogs records have increased significantly since 2017. This can be seen in the graph earthquake cumulative number (Figure 8).

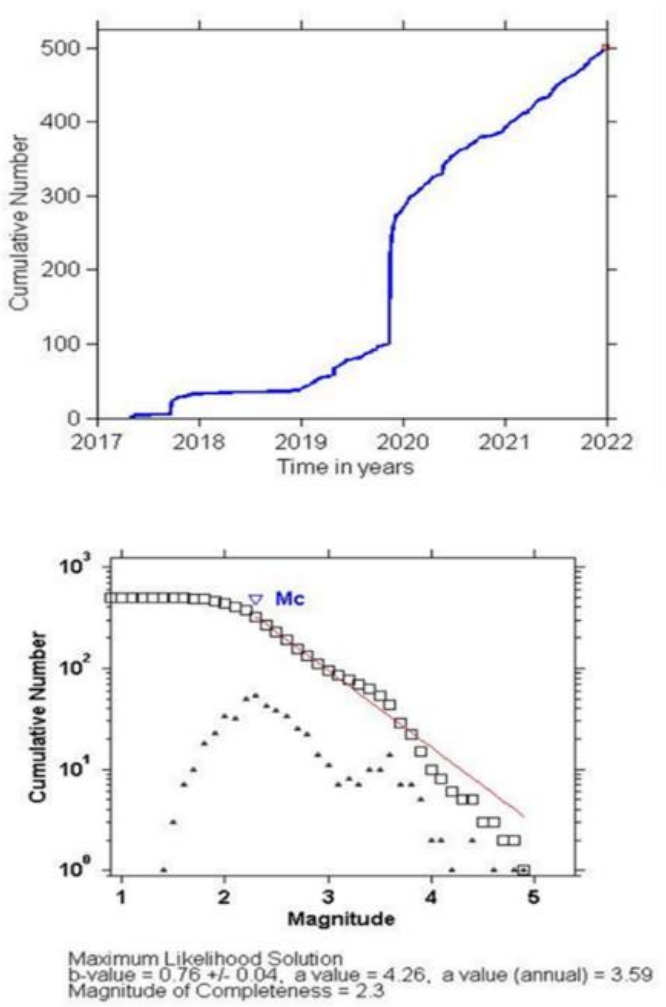

Figure 8. Cumulative number of earthquakes in Bali from 2017-2021 (top) and frequency distribution magnitude of the earthquake in Bali 1963-2021 (bottom). (Source: Earthquake Catalog Processing Result, 2022)

Based on IAEA (2016), earthquakes are classified into two groups: earthquakes occurring on identified seismotectonic structures and earthquakes occurring in locations where no apparent correlation can be made with any specific geological structure, referred to as diffuse seismicity. From the 5 km buffer analysis using the fault

analysis of the PALSAR-2, obtained 37 diffuse earthquakes. When the fault is combined with the spots from the geological map and PALSAR-2 lineaments, the diffuse earthquakes become 32 events. Diffuse earthquakes are caused by unidentified faults or ellipsoid errors in determining earthquake epicenters. For small-magnitude earthquakes, location errors depend on the geometry and noise levels of the stations that make up the network (D'Alessandro & Stickney, 2012).

Based on geographics and the direction of the strikes (Figure 9), there are indications that the Pesanggaran Fault and Sepang Fault are extensions of the East Coast Fault and Pajahan Fault, respectively. Banyuwedang and Tegal Badeng faults are related to earthquake history, and specifically for Banyuwedang, there is also a hot spring in that area.

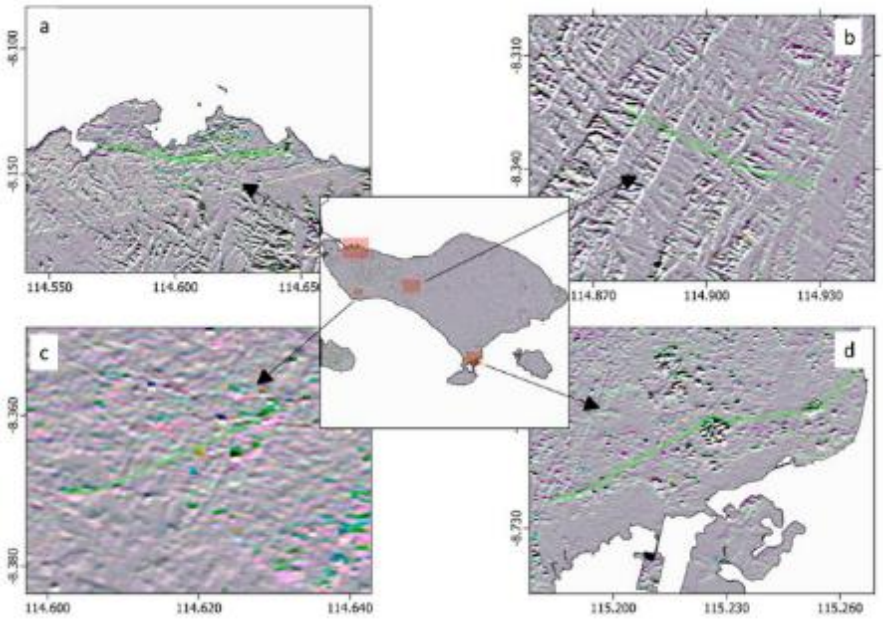

Figure 9. New fault identification showing characteristic textural signatures of different lithological facies in the directional filter (a. Banyuwedang, b. Sepang, c. Tegal Badeng, and d. Pesanggaran) (Source: Data Processing Result, 2022).

Some regions show a gap morphological condition, which indicates weak zones, weak zones, or non-resistance is also equal to the distribution of fault patterns and earthquake points. (Wijay et al., 2020) made observations of outcrop in Bubunan, Singaraja, an andesitic intrusion part of the Jembrana Volcanic Rock Formation. From their observations, a morphological displacement where the andesite intrusion body is cut off and moved away from each other is still part of the Busungbiu fault pattern Busungbiu fault kinematically has a left slip movement. Horizontal fault traces form a negative flower structure pattern in the alluvium outcrop.

(Astra et al., 2014) interpreting in the western region of Buleleng resulted in an ascending fault model in which the SVD value on the minimum curve is more dominant than the maximum curve value but did not mention the fault name. We estimated this fault between the Seririt fault and Renon Mt Fault, and the results in this study resulted in both thrust faults. New spots identified using SAR data in the Banyuwedang area are related to the results study by (Purnomo & Pichler, 2015) that confirmed the fault-hosted geothermal system of Banyuwedang. (Agasty et al., 2022) conducted a field study for the identification of the Rendang fault using

tectonic geomorphological methods and geological mapping obtained lineament data collection totaling 141 lineaments with a dominant direction of northeast-southwest (NE-SW), where the presence of Mount Abang and Agung Volcano also controls fault patterns in the area. The length of the Rendang fault based on (Agasty et al., 2022) analysis is 18 km; this result is not far different from the lineament method using PALSAR-2 in this study, which is 18,5 km.

Indications of reactivation of the main fault on the East Coast of Bali are in the fluvial facies where a shear zone can be seen with a reverse fault mechanism N345°E/83° (Soehaimi et al., 2015; Ariantan et al., 2018). This result differs from the dip angle obtained from 3D modeling, which is 50°.

Based on the Probabilistic Seismic Hazard Analysis (PSHA) map for the Bali land (Pusgen, 2017; Pratama, 2020), the maximum value of earthquake ground acceleration is caused by the potential for earthquakes from the Flores Back Arc Thrust. The maximum intensity was caused by the 1976 sericite earthquake and the 1979 kidnapping earthquake, both felt at VII MMI (Soehaimi & Setiawan, 2014). However, some local active faults cause some damage with low magnitude (<5). Based on a survey of 14 GPS points throughout Bali from 2013 to 2015, The horizontal velocity of Bali GPS sites varies from 1.93 mm/year to 22.53 mm/year in the NE direction. In contrast, the vertical rate ranges between -184.34 mm/year to 33.79 mm/year (Sulaiman et al., 2018). The relative velocity may associate with the tectonic activity due to the subduction at southern Bali, West Flores Back-Arc Thrust, and East Flores Back-Arc Thrust at the northern part; and Lombok Strait Fault and a fault at eastern Bali with magnitude (Mw) 7.1, 6.6, 6.8, 5.8, and 5.2, respectively.

This study proposes 30 faults in Bali, including 26 spots from geological maps with changes in length and location shift and four new areas extracted from semi-automatic contour (Figure 10). The combination of gravity and SAR data can interpret faults well. However, more historical earthquake data is needed. Considering the current sensors, earthquake recording only takes time so that the fault zone will be identified appropriately. The observed image results are improving through the development of increasingly sophisticated remote sensing technology.

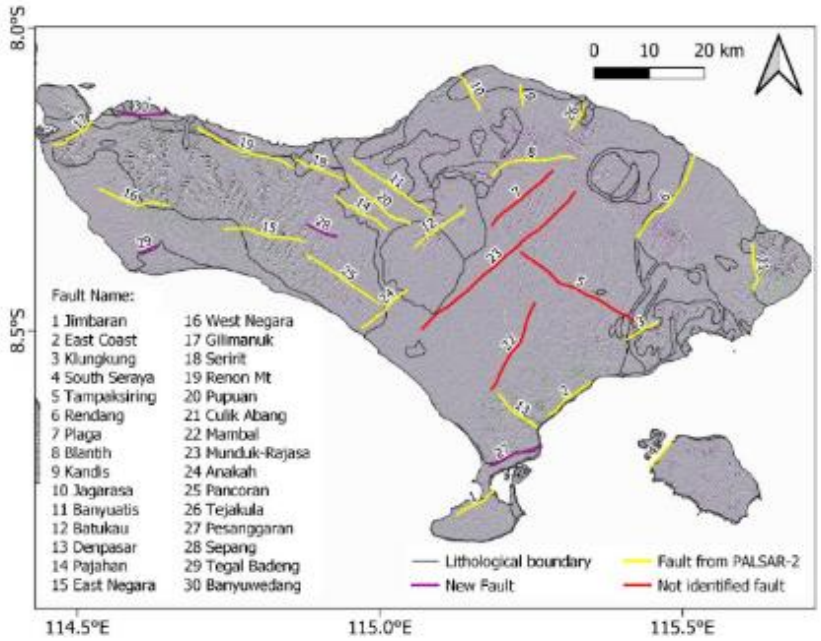

Figure 10. Fault identification results in Bali using GGMPlus Gravity and ALOS-2 PALSAR-2 data. (Source: Data Processing Result, 2022).

This study highlighted the importance of the satellite data from the GGMPlus and ALOS-2 PALSAR-2 data combination and the proposed methodology to enhance geological features for mapping fault zone, particularly in Bali land. The results of automatic lineage analysis with the PCI Geomatica LINE module resulted in the identification of lineaments mainly in the western part of Bali, following (Helmi et al., 2021) research results obtained a lineament delineation in a northwest-southeast (NW-SE) direction. This is due to differences in the data and lineament extraction method used.

Previous research on the identification of active faults on Bali land used DEM data by (Helmi et al., 2021), using gravity data by (Astra et al., 2014), and (Wijaya et al., 2020). However, the three studies did not do the research for the entire Bali area and with limited data. The results of this study provide a new understanding of the geometry of active faults on the island of Bali and the potential for future earthquakes to contribute to earthquake disaster mitigation efforts on the island of Bali. With the improvement in the quality of earthquake records, seen from the decrease in the value of Mc, it is stated that more small earthquakes can be adequately analyzed, thus increasing the number of historical earthquake catalogs available. Socializing potential fault hazards and earthquake risks to local communities and stakeholders in earthquake mitigation is necessary. Settlements (buildings, houses) must strictly follow the building code based on the acceleration value and local soil conditions.

Remote sensing data for geological lineament mapping leads to determining the faults and tectonic implications by substituting conventional methods. Geological lineament extraction is directly associated with the interpreter's skill, experience, and remote sensing data (Ahmadi & Pekkan, 2021).

Identification of active fault traces in Bali land has provided high disaster risks. We hope this study can properly mitigate and provide stakeholders with input about the threat of earthquakes due to local faults. In the future, we need to increase the awareness of shallow earthquakes of medium-high magnitude because they can endanger residents around this fault zone, especially residents who live in houses or buildings that are not earthquake-resistant. Socialization about potential hazards and earthquake mitigation needs to be improved, especially in fault zones.

CONCLUSION

This study proposes 30 faults in Bali, including 26 spots from geological maps with changes in length and location shift and four new areas extracted from semi-automatic lineament. Places in Bali land are controlled by subduction in the south of the island of Bali, between the Eurasian Continent Plate and the Indo-Australian Ocean Plate. Some spots are in the contact area of the lithological boundary, and the rest intersect the lithological boundary. Based on the age of the rock formations, these faults pass through with the age of the Quaternary rocks. All of these faults are categorized as active faults. All spots are associated with at least one earthquake occurrence and have the same fault type as their focal mechanism.

Various methods of determining faults must be carried out to ensure each fault parameter has straightforward measurements in the field. In the future, it is necessary to be aware of shallow earthquakes of medium-high magnitude because they can endanger residents around this fault zone, especially residents who live in houses or buildings that are not earthquake-resistant.

ACKNOWLEDGMENT

We thank the parties who provided the data used in this research: JAXA for ALOS-2 PALSAR-2 Data, Curtin University for GGMPlus Data, Indonesian Agency for Meteorology Climatology and Geophysics (BMKG) for the earthquake catalog, Geological Agency of Indonesia for Bali

sheet geological map, and Indonesian Geospatial Information Agency (BIG) for DEMNAS data.

REFERENCE LIST

Agastya, I B. O., Diwyastra, P. D., & Hespiantoro, S. (2022). Identifikasi Zona Sesar Menggunakan Pendekatan Geomorfologi Tektonik dan Pemetaan Geologi di Desa Ban, Kabupaten Karangasem, Bali. Jurnal Geominerba 7(1), p. 14-25.

Ahmadi, H. & Pekkan, E. (2021). Fault-Based Geological Lineaments Extraction Using Remote Sensing and GIS—A Review. Geosciences, 11, 183. https://doi.org/10.3390/geosciences 11050183.

Aoki, Y., Furuya, M., De Zan, F. et al. (2021). L-band Synthetic Aperture Radar: Current and future applications to Earth sciences. Earth Planets Space 73(56). https://doi.org/10.1186/s40623-021-01363-x.

Ariantana, K., Agastya, I. B. O., Pradana, A. A., & Prameswari, M. D. 2018. Potential of Geological Natural Tourism in Hidden Canyon, Guwang Beji Village, Gianyar District, Bali Province. Proceedings Pekan Ilmiah Tahunan IAGI.

Astra, I M. K. A., Suarbawa, K. N., & Nugroho, H. A. (2014). Interpretasi Struktur Bawah Permukaan Sesar Lokal di Wilayah Singaraja- Bali Menggunakan Analisis Second Vertical Derivative. Megasains 5 (1), p. 49-55.

Bannari, A., El-Battay, A., Saquaque, A. & Miri, A. (2016). PALSAR-FBS L-HH Mode and Landsat-TM Data Fusion for Geological Mapping. Advances in Remote Sensing, 5, p. 246-268. http://dx.doi.org/10.4236/ars.2016.54020.

Camacho, M. and Alvarez, R. (2021). Geophysical Modeling with Satellite Gravity Data: Eigen-6C4 vs. GGM Plus. Engineering, 13, p. 690-706. https://doi.org/10.4236/eng.2021.1312050

Canny, J. (1986). A Computational Approach to Edge Detection. IEEE Transactions on Pattern Analysis and Machine Intelligence 8(6), p. 679–698. https://doi.org/10.1109/TPAMI.1986.4767851

Choi, S., Ryu, I., Lee, Y. C., & Son, Y. 2020. Gravity and magnetic field interpretation to detect deep buried paleo basinal fault lines contributing to intraplate earthquakes: a case study from Pohang Basin, SE Korea, Geophysical Journal International, Volume 220, p. 490–500, https://doi.org/10.1093/gji/ggz464.

D'Alessandro, A., & Stickney, M. 2012. Montana Seismic Network Performance: An Evaluation through the SNES Method. Bulletin of the Seismological Society of America, 102(1), p. 73–87. https://doi.org/10.1785/0120100234

Fitriyani, J., Apriyadi, R. K., Winugroho, T., Hartono, D., Widana, I D. K. K., & Wilopo. (2021). Karakteristik Histori Bencana Indonesia Periode 1815 – 2019 Berdasarkan Jumlah Bencana, Kematian, Keterpaparan dan Kerusakan Rumah Akibat Bencana. Journal of Science Education 5(3), p. 322-327, https://doi.org/10.33369/pendipa.5.3.322-327.

Ghosh, S., Sivasankar, T., & Anand, G. (2021). Performance evaluation of multi-parametric synthetic aperture radar data for geological lineament extraction. International Journal of Remote Sensing, 42:7, p. 2574-2593, https://doi.org/10.1080/01431161.2020.1856963

Ghosh, T., Hazra, S., & Kumar Das, A. (2022). Potential of ALOS-2 PALSAR-2 StripMap data for lithofacies identification and geological lineament mapping in vegetated fold-

thrust belt of Nagaland, India. Advances in Space Research 69(4), p. 1840–186. https://doi.org/10.1016/j.asr.2021.09.007.

Hadiwidjojo, M. M. P., Samodra, H., & Amin, T. C. 1998. Geological Map of The Bali Sheet, Nusa Tenggara, second edition. Geological Research and Development Cente of Indonesia.

Helmi, H., Marliyani, G. I., Nur'aini, S. (2021). Identifikasi Sesar Aktif di Pulau Bali dengan Menggunakan Data Pemetaan Geologi Permukaan dan Morfologi Tektonik. Majalah Geografi Indonesia 35(1), p. 45-53. ISSN 2540-945X. http://dx.doi.org/10.22146/mgi.61928.

Hirt, C, S.J. Claessens, T. Fecher, M. Kuhn, R. Pail, M. Rexer. (2013). New ultra-high resolutions picture of 2 Earth's gravity field, Geophysical Research Letters, Vol 40, https://doi.org/10.1002/grl.50838.

Hirt, C. 2013b. RTM gravity forward-modeling using topography/bathymetry data to improve high-degree global geopotential models in the coastal zone, Marine Geodesy 36(2), p. 1–20, https://doi.org/10.1080/01490419.2013.779334.

Hirt C., M. Kuhn, S.J. Claessens, R. Pail, K. Seitz, T. Gruber. 2014. Study of the Earth's short-scale gravity field using the ERTM2160 gravity model. Computers & Geosciences, 73, p. 71-80, doi: 10.1016/j.cageo.2014.09.00.

IAEA. 2016. Diffuse Seismicity in Seismic Hazard Assessment for Site Evaluation of Nuclear Installations, Safety Reports Series No. 89. International Atomic Energy Agency, Vienna, Austria.

Iswari, M. Y. & Anggraini, K. 2018. DEMNAS: Model Digital Ketinggian Nasional untuk Aplikasi Kepesisiran. Oseana 28(4), p. 68-80. https://doi.org/10.14203/oseana.2018.Vol.43No.4.2

JAXA. 2008. ALOS Data Users Handbook Revision C. Earth Observation Research and Application Center, Japan Aerospace Exploration Agency.

JAXA. 2014. ALOS-2/PALSAR-2 Level 1.1/1.5/2.1/3.1 CEOS SAR Product Format Description, Japan Aerospace Exploration Agency.

JAXA. (2022). PALSAR-2. Available in URL: https://www.eorc.jaxa.jp/ALOS/en/alos-2/a2_sensor_e.htm accessed July 19, 2022.

Jensen, J. R. (2015). Introductory Digital Image Processing: A Remote Sensing Perspective, 4th ed. Prentice-Hall, Englewood Cliffs.

Ming Y, Ma G, Li L, Han J, Wang T. 2021. The Spatial Different Order Derivative Method of Gravity and Magnetic Anomalies for Source Distribution Inversion. Remote Sensing 13(5):964. https://doi.org/10.3390/rs13050964

Pour, A.B. & Hashim, M. (2015). Structural mapping using PALSAR data in the Central Gold Belt, Peninsular Malaysia. Ore Geology Reviews, Vol. 64, P. 13-22, ISSN 0169-1368, https://doi.org/10.1016/j.oregeorev.2014.06.011

Pour, A. B. & Hashim, M. (2016). Geological Features Mapping Using Palsar-2 Data in Kelantan River Basin, Peninsular Malaysia. Int. Arch. Photogramm. Remote Sens. Spatial Inf. Sci., XLII-4/W1, 65–70, https://doi.org/10.5194/isprs-archives-XLII-4-W1-65-2016.

Pratama, I P. D. (2020). Pemetaan dan Analisis Probabilistic Seismic Hazard Analysis (PSHA) Radius 500 km dari Denpasar. Jurnal Geografi GEA 20(1), p. 54-62. https://doi.org/10.17509/gea.v20i1.23299

Purnomo, B. J. & Pichler, T. (2015). Geothermal systems on the island of Bali, Indonesia. Journal of Volcanology and Geothermal

Research, 304, p. 349-358. https://doi.org/10.1016/j.jvolgeores.2015.09.016

PuSGeN. 2017. Peta Sumber Daya dan Bahaya Gempa Indonesia Tahun 2017. Pustlitbang PUPR.

Soehaimi, A., Setiawan, J. H., & Marjiyono. (2014). Seismotectonic and Active Faults of Bali Island. 5th International INQUA Meeting on Paleoseismology, Active Tectonics and Archeoseismology (PATA), Busan, Korea.

Soehaimi, A., & Setianegara, R. (2015). Active Fault Study in the Eastern Coast of Bali Island, Indonesia. 6th International INQUA Meeting on Paleoseismology, Active Tectonics and Archeoseismology (PATA), Pescina, Funcino Basin, Italy.

Sulaeman, C., Hidayati, S., Omang, A., & Priambodo, I.C. (2018). Tectonic Model of Bali Island Inferred from GPS Data. Indonesian Journal on Geoscience, 5 (1), p. 81-91. https://doi.org/10.17014/ijog.5.1.81-91

Sumintadireja, P., Dahrin, D., & Grandis, H. 2018. A Note on the Use of the Second Vertical Derivative (SVD) of Gravity Data with Reference to Indonesian Cases. J. Eng. Technol. Sci., Vol. 50, No. 1, p. 127-139, https://doi.org/10.5614/j.eng.technol.sci.2018.50.1.9

Suprianto, A., Supriyadi, Priyantari, N., & Cahyono, E. B. (2021). Correlation Between GGMPlus, Topex and BGI Gravity Data in Volcanic Areas of Java Island. Journal of Physics: Conference Series. 1825. 012023. https://doi.org/10.1088/1742-6596/1825/1/012023.

Telford, W., Geldart, L. P. & Sheriff, R. 2004. Applied Geophysics, Second Edition. Cambridge: Cambridge University Press.

Ustinov, S., Ostapchuk, A., Svecherevskiy, A., Usachev, A., Gridin, G., Grigor'eva, A., & Nafigin, I. 2022. Prospects of Geoinformatics in Analyzing Spatial Heterogeneities of Microstructural Properties of a Tectonic Fault. Appl. Sci.12, 2864. https://doi.org/10.3390/app12062864

Veci, L. (2015). ALOS PALSAR Orthorectification Tutorial. Array Sistema Computing Inc.: North York, ON, Canada.

Verstappen, H. 2010. Indonesian Landforms and Plate Tectonics. Indonesian Journal on Geoscience 5(3). https://doi.org/10.17014/ijog.v5i3.103.

Wiemer, S. (2001). A Software Package to Analyze Seismicity: ZMAP. Seismological Research Letters, 72, p. 373-382, http://dx.doi.org/10.1785/gssrl.72.3.373

Wijaya, P. A., Agastya, I. B. O., & Satya, Y. (2020). Identification of Busungbiu Fault Zone from Gravity Data, Earthquake Data, and Geological Approach. The 45th Annual Scientific Meeting of Himpunan Ahli Geofisika Indonesia.

Yan, J., Chen, X., Meng, G., Lü, Q., Deng, Z., Qi, G., & Tang, H. 2019. Concealed faults and intrusions identification based on multiscale edge detection and 3D inversion of gravity and magnetic data: A case study in Qiongheba area, Xinjiang, Northwest China. Interpretation. 7(2)T331–T345. doi: https://doi.org/10.1190/INT-2018-0066.1

Yeomans, C. M., Middleton, M., Shail, R. K., Grebby, S., & Lusty, P. A. J. 2019. Integrated Object-Based Image Analysis for semi-automated geological lineament detection in southwest England, Computers & Geosciences, Vol. 123, pp. 137-148, ISSN 0098-3004, https://doi.org/10.1016/j.cageo.2018.11.005.